^{18}F-FNDP for PET Imaging of Soluble Epoxide Hydrolase

Andrew G. Horti[1], Yuchuan Wang[1], Il Minn[1], Xi Lan[2], Jian Wang[2], Raymond C. Koehler[2], Nabil J. Alkayed[3], Robert F. Dannals[1], and Martin G. Pomper[1]

[1]*Russell H. Morgan Department of Radiology and Radiological Science, Johns Hopkins Medical Institutions, Baltimore, Maryland;* [2]*Department of Neurology, Anesthesiology & Critical Care Medicine, Johns Hopkins Medical Institutions, Baltimore, Maryland; and* [3]*Department of Anesthesiology & Perioperative Medicine, Knight Cardiovascular Institute, Oregon Health & Science University, Portland, Oregon*

Soluble epoxide hydrolase (sEH) is a bifunctional enzyme located within cytosol and peroxisomes that converts epoxides to the corresponding diols and hydrolyzes phosphate monoesters. It serves to inactivate epoxyeicosatrienoic acids (EETs), which are generated in the brain to couple neuronal activity and cerebral blood flow in normal and pathologic states. Altered regulation of sEH was observed previously in various neuropathologic disorders including vascular dementia and stroke. Inhibitors of sEH are pursued as agents to mitigate neuronal damage after stroke. We developed *N*-(3,3-diphenylpropyl)-6-^{18}F-fluoronicotinamide (^{18}F-FNDP), which proved highly specific for imaging of sEH in the mouse and nonhuman primate brain with PET. **Methods:** ^{18}F-FNDP was synthesized from the corresponding bromo precursor. sEH inhibitory activity of ^{18}F-FNDP was measured using an sEH inhibitor screening assay kit. Biodistribution was undertaken in CD-1 mice. Binding specificity was assayed in CD-1 and sEH knock-out mice and *Papio anubis* (baboon) through pretreatment with an sEH inhibitor to block sEH binding. Dynamic PET imaging with arterial blood sampling was performed in 3 baboons, with regional tracer binding quantified using distribution volume. The metabolism of ^{18}F-FNDP in baboons was assessed using high-performance liquid chromatography. **Results:** ^{18}F-FNDP (inhibition binding affinity constant, 1.73 nM) was prepared in 1 step in a radiochemical yield of 14% ± 7%, specific radioactivity in the range of 888–3,774 GBq/μmol, and a radiochemical purity greater than 99% using an automatic radiosynthesis module. The time of preparation was about 75 min. In CD-1 mice, regional uptake followed the pattern of striatum > cortex > hippocampus > cerebellum, consistent with the known brain distribution of sEH, with 5.2% injected dose per gram of tissue at peak uptake. Blockade of 80%–90% was demonstrated in all brain regions. Minimal radiotracer uptake was present in sEH knock-out mice. PET baboon brain distribution paralleled that seen in mouse, with a marked blockade (95%) noted in all regions indicating sEH-mediated uptake of ^{18}F-FNDP. Two hydrophilic metabolites were identified, with 20% parent compound present at 90 min after injection in baboon plasma. **Conclusion:** ^{18}F-FNDP can be synthesized in suitable radiochemical yield and high specific radioactivity and purity. In vivo imaging experiments demonstrated that ^{18}F-FNDP targeted sEH in murine and nonhuman primate brain specifically. ^{18}F-FNDP is a promising PET radiotracer likely to be useful for understanding the role of sEH in a variety of conditions affecting the central nervous system.

Received Jan. 26, 2016; revision accepted May 16, 2016.

For correspondence or reprints contact either of the following:
Martin G. Pomper, Johns Hopkins Medical School, 1550 Orleans St., 492 CRB II, Baltimore, MD 21287.
E-mail: mpomper1@jh.edu
Andrew G. Horti, Johns Hopkins University School of Medicine, 600 North Wolfe St., Nelson B1-122, Baltimore, MD 21287-0816.
E-mail: ahorti1@jhmi.edu

Published online Jul. 14, 2016.

Key Words: soluble epoxide hydrolase; positron emission tomography; stroke; vascular cognitive impairment; baboon; epoxyeicosatrienoic acid; molecular neuroimaging

J Nucl Med 2016; 57:1817–1822
DOI: 10.2967/jnumed.116.173245

Epoxyeicosatrienoic acids (EETs) are signaling molecules important in the vasodilation of cerebral vessels that accompanies neuronal activity. They also modulate the activity of numerous molecular targets and signaling pathways (*1*). Soluble epoxide hydrolase (sEH), abundantly distributed throughout the mammalian body (*2,3*), catalyzes the hydrolysis of EETs to less biologically active molecules (*4*). During the last decade, sEH has become a pharmaceutical target, and several small-molecule sEH inhibitors have been developed. Those sEH inhibitors elevate levels of EETs that in turn could benefit a variety of conditions including hypertension, atherosclerosis, inflammation, diabetes, pain, and pulmonary diseases, among others (*5*).

Regulation of sEH is altered in many conditions, including vascular cognitive impairment (VCI) and stroke. The contribution of cerebrovascular pathology to Alzheimer disease (AD) and dementia is becoming more appreciated. Postmortem studies have shown that one third of patients with dementia have comorbid cerebrovascular pathology (*6,7*). A recent report found a 50% greater sEH activity in subjects with VCI versus age-matched controls (*8*). The most common type of VCI is associated with white matter hyperintensities that are early predictors of conversion to mild cognitive impairment (*8*) that, in turn, represents an increased risk of developing AD.

As noted above, changes in the expression of sEH alter the biologic effects of EETs. A consistently observed effect of EETs is their ability to prevent apoptosis after ischemic insult as well as other forms of injury (*9*). Various studies have shown that EETs protect the brain during stroke and that inhibition of sEH enhances this effect (*10*). Patients suffering aneurysmal subarachnoid hemorrhage are at high risk for delayed cerebral ischemia and stroke (*11*). Patients with the common K55R genetic polymorphism in the sEH gene (*Ephx2*) demonstrated 30% lower levels of EETs due to increased activity of sEH (*12*), and they exhibited a mortality of 28.6% after stroke versus 5.3% in the control subjects (*11*). Other studies have demonstrated highly increased expression of sEH in animal models of epilepsy (*13*) and Parkinson disease (*14*).

In addition to facilitating drug development (*5*), the importance of a PET imaging agent targeting sEH resides in gaining a better understanding of stroke and dementia, namely the vascular aspects

of the latter, noninvasively, repeatedly and at high resolution. Clinically, stroke is evaluated primarily through anatomic and functional MRI, with molecular approaches limited because of a lack of viable radiotracers for this indication beyond those used to measure perfusion with SPECT (*15*). A PET agent for sEH may enable distinction between AD and VCI in vivo, rather than having to rely on postmortem observation of Aβ plaques and neurofibrillary tangles (*16,17*).

Here we describe the synthesis (Fig. 1), rodent biodistribution, and baboon brain PET imaging of *N*-(3,3-diphenylpropyl)-6-^{18}F-fluoronicotinamide (^{18}F-FNDP), a radiotracer for sEH that is structurally similar to the potent sEH inhibitor *N*-(3,3-diphenylpropyl)-nicotinamide (*18*) (nor-fluoro-FNDP).

MATERIALS AND METHODS

The experimental animal protocols were approved by the Animal Care and Use Committee of the Johns Hopkins Medical Institutions.

Chemistry

Synthesis of *N*-(3,3-diphenylpropyl)-6-fluoronicotinamide (FNDP) and 6-bromo-*N*-(3,3-diphenylpropyl)nicotinamide (precursor-FNDP) is described in the supplemental materials (available at http://jnm.snmjournals.org).

^{18}F-FNDP. A solution of ^{18}F-fluoride obtained from proton bombardment of ^{18}O-water in a PETtrace cyclotron (GE Healthcare) and 2 mg of K_2CO_3 in 0.4 mL of water and 15–20 mg of Kryptofix 222 (Sigma-Aldrich) in 2 mL acetonitrile were added to a reaction vessel of a MicroLab module (GE Healthcare). The mixture was evaporated azeotropically at 140°C under a stream of argon after the addition of 2 mL of CH_3CN. A solution of the precursor-FNDP (2 mg) in dimethyl sulfoxide (0.8 mL) was added to the reaction vessel with the mixture heated at 160°C for 12 min. The reaction mixture was cooled, diluted with 0.7 mL of water, and injected onto the reversed-phase semipreparative high-performance liquid chromatography (HPLC) column. The radioactive product peak was collected in 50 mL of HPLC-grade water. The water solution was transferred through an activated Waters C-18 Sep-Pak light cartridge. After the cartridge was washed with 10 mL of saline, the product was eluted with 1 mL of ethanol through a 0.2-μM sterile filter into a sterile, pyrogen-free vial, and 10 mL of 0.9% saline were added through the same filter. The final product ^{18}F-FNDP was then analyzed by analytic HPLC to determine the radiochemical purity and specific radioactivity. The total preparation time including quality control was 75 min.

Semipreparative HPLC Conditions

The following were semipreparative HPLC conditions: Luna C18, 10 μm, 10 × 250 mm; mobile phase, 45:55 (acetonitrile, 0.1 M aqueous ammonium formate); flow rate, 10 mL/min; ultraviolet, 254 nm; retention time, 13 and 21 min (FNDP and precursor-FNDP, respectively).

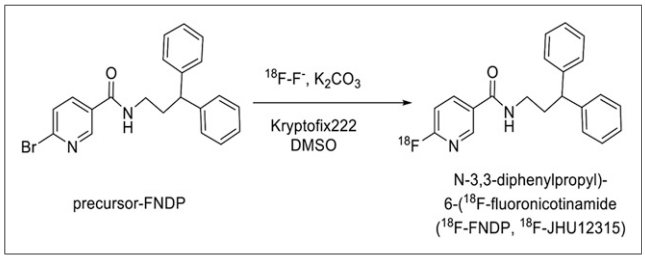

FIGURE 1. Radiosynthesis of ^{18}F-FNDP, a radiotracer for PET imaging of sEH.

Analytic HPLC Conditions

The following were analytic HPLC conditions: Luna C18, 10 μm, 4.6 × 250 mm; mobile phase, 55:45 (acetonitrile, 0.1 M aqueous ammonium formate); flow rate, 3 mL/min; ultraviolet, 254 nm; retention time, 3.9 and 6.5 min (FNDP and precursor-FNDP, respectively).

In Vitro Inhibition of sEH with FNDP

Inhibitory activity of FNDP and nor-fluoro-FNDP, an analog of FNDP and known inhibitor of sEH (*18*), was measured using the sEH Inhibitor Assay Kit (Cayman Chemical). In brief, half maximal inhibitory concentration (IC_{50}) values of the sEH inhibitors were determined by measuring the inhibition of hydrolysis of (3-phenyl-oxiranyl)-acetic acid cyano-(6-methoxy-naphthalen-2-yl)-methyl ester by sEH. AUDA (Cayman Chemical), a known inhibitor of sEH (*19*), was used as a positive control. All reactions were done in triplicate, and the data were analyzed using GraphPad Prism (GraphPad Software) and inhibitory constants (inhibition binding affinity constant [K_i] values) were generated.

Biodistribution Studies with ^{18}F-FNDP in Mice

Baseline Study in CD-1 Mice. Male, CD-1 mice weighing 25–27 g from Charles River were used. The animals were sacrificed by cervical dislocation at 5, 15, 30, 60, and 90 min after injection of 3.7 MBq (0.1 mCi) of ^{18}F-FNDP (specific radioactivity, 814 GBq/μmol [22,000 mCi/μmol]) in 0.2 mL of saline into a lateral tail vein (n = 3). The brains were removed and dissected on ice. Striatum, cortex, hippocampus, hypothalamus, cerebellum, and the rest of the brain were weighed, and their radioactivity content was determined in a γ-counter LKB/Wallac 1283 CompuGamma CS (Perkin Elmer). Aliquots of the injectate were prepared as standards, and their radioactivity content was determined along with the tissue samples. The percentage injected dose per gram of tissue (%ID/g of tissue) was calculated.

Blocking of ^{18}F-FNDP Binding in CD-1 Mice. In vivo binding specificity (blocking) studies were performed by subcutaneous administration of various doses (0, 0.03, 0.3, 1, and 3 mg/kg) of nor-fluoro-FNDP followed by intravenous injection of 3.7 MBq (0.1 mCi) of ^{18}F-FNDP 15 min thereafter (n = 3). Ninety minutes after administration of the radiotracer, the animals were sacrificed by cervical dislocation, brain tissues were harvested, and their radioactivity content was determined.

Baseline and Blocking Studies of ^{18}F-FNDP in sEH Knock-Out (sEH-KO) and C57BL/6 Control Mice

Baseline and blockade studies (nor-fluoro-FNDP, 1 mg/kg, subcutaneously) with the same batch of ^{18}F-FNDP were performed similarly to the studies described above. sEH-KO mice (*Ephx2* gene deletion; Jackson Laboratory) and C57BL/6 background strain mice were studied. Animals were sacrificed at 60 min after radiotracer injection.

The sample size of CD-1 and sEH-KO mice in the baseline and blocking studies was 3 and 5, respectively, corresponding to the statistical power value greater than 0.9 as calculated by G*Power, v.3.1.9.2 freeware.

Baboon PET and Radiometabolite Studies (Supplemental Materials)

Dynamic baseline PET experiments (90 min) were performed on 3 male baboons (*Papio anubis*) weighing 23.9, 25.0, and 28.2 kg, using the High Resolution Research Tomograph (HRRT; CPS Innovations, Inc.). A blocking PET scan was also conducted with the last of the baboons. In brief, the baseline dynamic PET acquisitions were performed with an intravenous injection of 290 ± 37 MBq (7.9 ± 1.0 mCi) of ^{18}F-FNDP (specific radioactivity, 1,521 ± 1,020 GBq/μmol [41,107 ± 27,579 mCi/μmol]; carrier mass, 0.004 ± 0.002 μg/kg). For the blocking study, nor-fluoro-FNDP (2 mg/kg) was given subcutaneously 1 h before the intravenous bolus injection of 307 MBq (8.3 mCi) of ^{18}F-FNDP (specific radioactivity, 1420 GBq/μmol [38,386 mCi/μmol]; carrier mass, 0.0025 μg/kg) and the start of the dynamic scan. Radiometabolite

analysis in baboon arterial blood was performed under the general conditions published previously (*20*) and are described in detail in the supplemental materials.

PET Data Analysis

PET image reconstruction, volumes of interest and regional time–activity curves, and PET kinetic analysis, which involved calculation of brain regional distribution volume (V_T), are described in the supplemental materials.

RESULTS

Chemistry

N-(3,3-diphenylpropyl)-6-fluoronicotinamide (FNDP) and *N*-(3,3-diphenylpropyl)-6-bromonicotinamide (precursor-FNDP) were synthesized with high yield (59%–72%) (supplemental materials; Supplemental Fig. 1). The molecular structures of FNDP and precursor-FNDP were confirmed by nuclear magnetic resonance analysis.

^{18}F-FNDP was prepared by nucleophilic radiofluorination of the bromo precursor-FNDP in a radiochemical yield of 14% ± 7% (n = 6) (non–decay-corrected), specific radioactivity in the range of 888–3,774 GBq/mmol (24,000–102,000 mCi/μmol) at the time synthesis ended, and in a radiochemical purity greater than 99% (Fig. 1). The final product, ^{18}F-FNDP, was formulated as a sterile, apyrogenic solution in 7% ethanolic saline with a pH of 5.5–6.5.

FNDP exhibited IC_{50} and K_i values comparable to the potent sEH inhibitor AUDA. IC_{50} values of FNDP, nor-fluoro-FNDP, and AUDA were 8.66 ± 0.06, 18.53 ± 0.04, and 6.48 ± 0.05 nM, respectively (Supplemental Fig. 2). The corresponding K_i values of FNDP, nor-fluoro-FNDP, and AUDA were 1.73, 3.71, and 1.30 nM, respectively.

Regional Brain Distribution Studies in CD-1 Mice

Baseline Study. The regional distribution of ^{18}F-FNDP in the CD-1 mouse brain is shown in Table 1.

sEH Binding Specificity of ^{18}F-FNDP: Dose-Escalation Blocking in CD-1 Mice. The sEH inhibitor nor-fluoro-FNDP blocked the ^{18}F-FNDP binding in all studied brain regions (striatum, hippocampus, cortex, and cerebellum) at 60 min after injection in a dose-dependent fashion (Fig. 2). At the highest blocker dose of 3 mg/kg, the reduction of radioactivity uptake in the striatum, hippocampus, and cortex was approximately 90% and in the cerebellum it was approximately 75%.

Baseline and Blocking Studies of ^{18}F-FNDP in sEH-KO and C57BL6 Control Mice. In the baseline experiment at 60 min after injection, the regional uptake of ^{18}F-FNDP in the C57BL6 control mice was approximately 1 %ID/g in the striatum, hippocampus, and cortex and 0.5 %ID/g in the cerebellum (Fig. 3). In the blocking experiment in the C57BL6 mice, the ^{18}F-FNDP brain uptake was reduced to approximately 0.2 %ID/g tissue in all regions studied. In sEH-KO mice, the regional brain uptake of ^{18}F-FNDP at 60 min was nearly the same in the baseline (0.11–0.12 %ID/g) and blocking experiments (0.10–0.11 %ID/g) (Fig. 3).

PET Imaging in *Papio Anubis*

High, heterogeneous uptake of radioactivity into the baboon brains was observed during baseline scans after bolus injection of ^{18}F-FNDP (Fig. 4). Regional time–activity curves peaked at approximately 5 min, with peak SUVs ranging from 2.5 to 4.0 g/mL. The SUV_{peak} of the entire brain was 3.2 and gradually reduced to 1.8 at 90 min. The highest accumulation of radioactivity occurred in the putamen, insula, frontal cortex, and amygdala, with lower uptake in white matter and cerebellum. Notably, time–activity curves of the cerebellum decreased more rapidly than for other regions (Fig. 4). For baseline scans, all brain regions yielded stable V_T estimates for scans longer than 60 min when using either compartmental modeling or Logan graphical analysis, where the 2 methods generated comparable regional V_T results (supplemental materials). To facilitate obtaining V_T parametric images, V_T values presented herein were based on the Logan method.

When quantified using V_T for baseline studies, among the 13 brain volumes of interest investigated, the highest radioligand binding occurred in the insula, putamen, caudate, and amygdala ($V_T >$ 11.5), with intermediate uptake in frontal/temporal gyrus and hippocampus ($V_T > 10.1$), followed by globus pallidus, corpus callosum, white matter, hypothalamus, and thalamus ($V_T > 8.1$). Lowest binding was in the cerebellum, with an average V_T of 7.9 ± 1.0.

Time–activity curve comparisons between baseline and blocking studies in the same baboon are shown in Figure 5. With blocking, regional time–activity curves peaked much earlier, at approximately 1 min after injection, with an average SUV_{peak} of 2.3 g/mL over the entire brain, and decreased rapidly to an average SUV of 0.18 g/mL, 10% of the baseline value, at the end of the 90-min scan. All regions in the blockade scan showed a $V_T < 0.8$ and reductions of > 90% when compared with baseline V_T values. The percentage reductions were comparable between high- and low-binding regions identified during the baseline study, for example, insula and amygdala at 95% reduction, whereas the cerebellum demonstrated 93% reduction (Supplemental Fig. 3). Parametric V_T images were generated for both baseline and blocking scans for comparison (Fig. 6).

The specific radioactivity of ^{18}F-FNDP doses in the blockade and baseline baboon studies ranged between 629 and 2,634 GBq/μmol. Because the specific activity was so high, the corresponding FNDP carrier mass was only 0.001–0.006 μg/kg, 6 orders of magnitude lower than the nor-fluoro-FNDP blocker dose (2 mg/kg). Therefore, variability in specific radioactivity unlikely affects the results.

TABLE 1
Regional Distribution of ^{18}F-FNDP in CD-1 Mouse Brain (Mean %ID/g Tissue ± SD, n = 3)

Brain region	5 min	15 min	30 min	60 min	90 min
Striatum	5.24 ± 0.45	3.29 ± 0.36	2.32 ± 0.15	1.07 ± 0.14	0.54 ± 0.07
Cortex	4.69 ± 0.21	2.92 ± 0.36	2.07 ± 0.05	0.87 ± 0.14	0.45 ± 0.05
Hippocampus	3.29 ± 0.54	2.51 ± 0.34	1.76 ± 0.15	0.81 ± 0.15	0.43 ± 0.06
Rest of brain	3.53 ± 0.11	2.37 ± 0.34	1.64 ± 0.06	0.71 ± 0.10	0.38 ± 0.04
Hypothalamus	2.59 ± 0.18	1.66 ± 0.28	1.04 ± 0.08	0.51 ± 0.07	0.31 ± 0.05
Cerebellum	2.75 ± 0.11	1.31 ± 1.01	1.09 ± 0.16	0.52 ± 0.07	0.29 ± 0.04

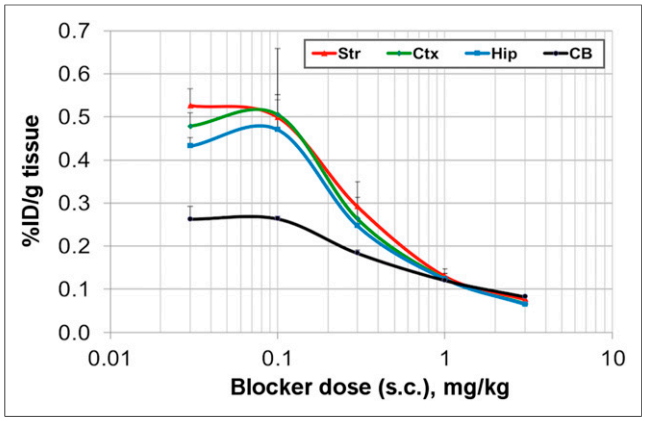

FIGURE 2. Dose-dependent blocking of ^{18}F-FNDP (3.7 MBq [0.1 mCi]) uptake with sEH inhibitor nor-fluoro-FNDP (s.c. [subcutaneously]) in CD-1 mouse brain at 60 min after radiotracer injection. Data are mean %ID/g tissue ± SD (n = 3). Blocking curve demonstrates that ^{18}F-FNDP specifically labels sEH binding sites in all brain regions studied. Residual binding at highest dose of blocker corresponds to nonspecific binding. CB = cerebellum; Ctx = cortex; Hip = hippocampus; Str = striatum.

Radiometabolite analysis of blood samples from baboons using reversed-phase HPLC showed that the parent compound ^{18}F-FNDP was metabolized to 2 hydrophilic species (Supplemental Fig. 6). The combined radiometabolites in the plasma reached values of 80% in baboons at 90 min after injection (Supplemental Figs. 5 and 6).

DISCUSSION

Because of the lack of available radiotracers, only about 39 of the hundreds of known binding sites (receptors and enzymes) in the human brain have been imaged by PET (*21*). Until now, sEH was one of many binding sites lacking a specific PET radiotracer.

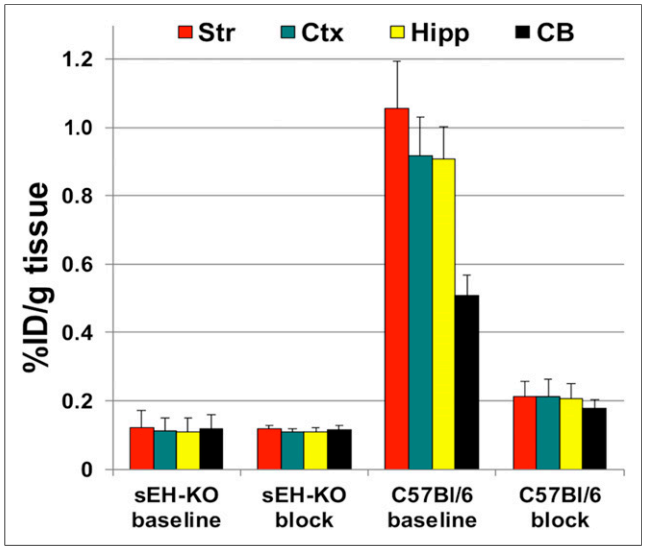

FIGURE 3. Baseline and blocking of ^{18}F-FNDP (3.7 MBq [0.1 mCi]) uptake in sEH-KO and control C57BL/6 mice at 60 min after injection of radiotracer. Data are mean %ID/g ± SD (n = 5). Blocking used sEH inhibitor nor-fluoro-FNDP (1 mg/kg, subcutaneously). CB = cerebellum; Ctx = cortex; Hipp = hippocampus; Str = striatum

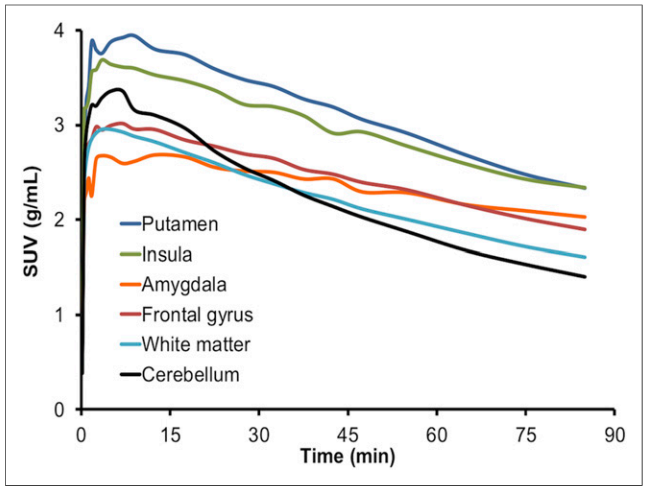

FIGURE 4. Representative time–activity curves obtained from baseline PET study in baboons. Thirteen brain regions were analyzed, 6 of which were shown above for clarity.

With the substantial number of sEH inhibitors developed by the pharmaceutical industry and academia, opportunities for sEH PET radiotracer development are available. However, many potent sEH inhibitors possess a large hydrophobic domain, rendering them unlikely radiotracers because of potentially high nonspecific binding (Supplemental Fig. 4).

Here we synthesized *N*-(3,3-diphenylpropyl)-6-fluoronicotinamide (FNDP; Supplemental Fig. 1), a potent sEH inhibitor with molecular properties (log P, 2.9; molecular weight, 334 Da) optimal for brain PET radiotracers (*22*). FNDP is structurally similar to the sEH inhibitor *N*-(3,3-diphenylpropyl)-nicotinamide (nor-fluoro-FNDP), identified by Boehringer Ingelheim as an sEH inhibitor (human IC_{50} of 7 nM) with improved druglike characteristics (*18*), and was used here as a lead compound for development of FNDP and blocker in animal experiments. In vitro assay demonstrated that FNDP is an sEH inhibitor with higher potency than that of the lead nor-fluoro-FNDP and comparable to the sEH inhibitor AUDA (supplemental materials; Supplemental Fig. 2).

FNDP contains a fluorine atom in position 2 of the pyridine ring that is activated for nucleophilic substitution and can be readily radiofluorinated via a corresponding bromo precursor (*23*). Radiosynthesis of ^{18}F-FNDP was performed in a conventional ^{18}F-FDG radiochemistry module by the nucleophilic radiofluorination of precursor-FNDP (Fig. 1) followed by semipreparative HPLC separation and formulation of the final radiolabeled product as a sterile apyrogenic solutions. The radiotracer was prepared with very-high-specific radioactivity and radiochemical purity. Precursor-FNDP was readily separated by preparative HPLC and was not detectable in the final product ^{18}F-FNDP by analytic HPLC.

Mouse Studies

In CD-1 mice, ^{18}F-FNDP exhibited a heterogeneous pattern of brain uptake, comparable to the expected regional expression of sEH in the mouse brain (*3*). Peak uptake was 5.2 %ID/g at 5 min after injection, followed by a rapid decline. That brain uptake is considered to be moderately high because uptake of 1 %ID/g has traditionally been used as the minimum criterion for selection of investigational central nervous system radiotracers at our PET center. Among brain regions studied, the highest accumulation of ^{18}F-FNDP occurred in the striatum, cortex, hippocampus, and

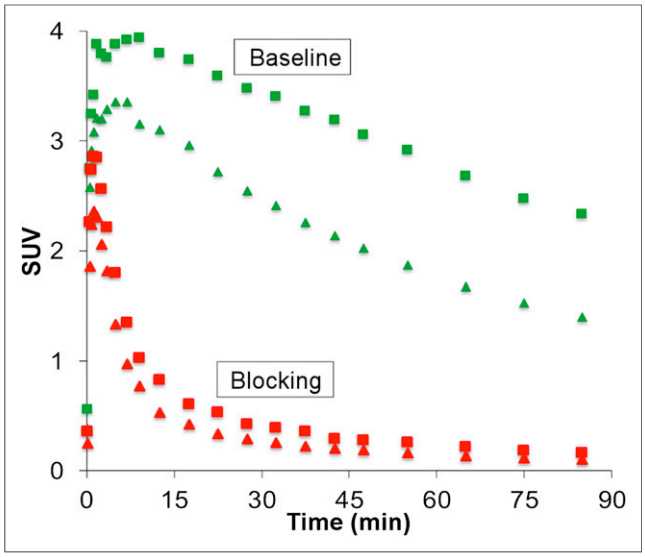

FIGURE 5. Comparison of regional time–uptake curves of ^{18}F-FNDP at baseline (green) and after blockade (red) with nor-fluoro-FNDP (2 mg/kg) in same baboon shows striking reduction of radioactivity in blocking scan. Two representative regions, putamen (squares) and cerebellum (triangles), are shown.

rest of brain, whereas lower but considerable radioactivity was seen in the hypothalamus and cerebellum (Table 1). The mouse brain distribution is comparable with in vitro data (*3*).

Two types of studies were performed for demonstration of the specificity of ^{18}F-FNDP binding, namely, dose-escalation blockade in CD-1 mice and biodistribution in sEH-KO mice. Regional brain uptake of ^{18}F-FNDP in CD-1 mice, a common strain for testing PET radiotracers, was highly sensitive to escalating doses of the sEH inhibitor nor-fluoro-FNDP (Fig. 2). The blocked binding in CD-1 mouse brain is considered to be specific (90% in the striatum, hippocampus, and cortex), whereas the residual binding at the high dose of the blocker is considered to be nonspecific binding (10%). These findings indicate that ^{18}F-FNDP uptake in the mouse brain is highly specific and mediated by sEH. The 75% blocking of radioactivity in the cerebellum is consistent with expression of sEH in this region (*3*) and suggests that the cerebellum may not be able to be used as a reference in the mouse brain.

As a further test of binding specificity, we used sEH-KO mice and control animals with the same genetic background (C57BL/6) (*24*). Because the sEH-KO mouse brain is devoid of sEH (*14*), we expected that ^{18}F-FNDP binding in these mice would be nonspecific and that the difference between sEH-KO and control brain uptake would represent specific sEH binding. Uptake of ^{18}F-FNDP was compared in the baseline experiments in sEH-KO and control animals (C57BL/6) at 60 min after radiotracer injection (Fig. 3). There was a marked reduction of ^{18}F-FNDP uptake (~90%) in the sEH-KO mice as compared with controls. High values of control/sEH-KO were demonstrated in all regions tested (10.3, striatum; 9.4, cortex; 9.2, hippocampus; 4.8, cerebellum). Furthermore, reduction of ^{18}F-FNDP uptake in sEH-KO mice was negligible in a blockade study using the sEH inhibitor nor-fluoro-FNDP (Fig. 3). That negligible effect indicated that any nonspecific binding of ^{18}F-FNDP to other proteins, such as the product of the *Ephx1* gene (microsomal epoxide hydrolase) (*3*), was negligible in the sEH-KO brain. In the C57BL/6 controls the blocking effect (~80%) (Fig. 3) proved similar to that in CD-1 mice (Fig. 2).

The mouse studies demonstrated that ^{18}F-FNDP readily entered the brain (5 %ID/g at peak) and labeled cerebral sEH in 2 strains of control mice (CD-1 and C57BL/6) with a high degree of specificity (80%–90%). In agreement with low expression of sEH in the KO animals, brain uptake of ^{18}F-FNDP in sEH-KO mice was 10-fold lower than that in the controls and is essentially nonspecific.

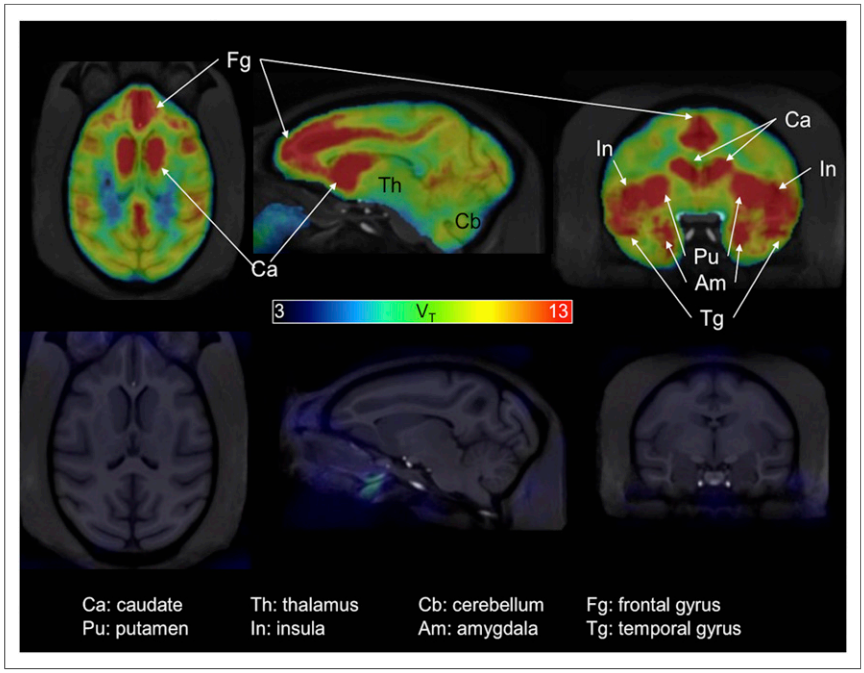

FIGURE 6. PET baseline (averaged, 3 scans, top) and blocking (single scan, bottom) parametric V_T images of ^{18}F-FNDP in baboon brain. PET images, displayed with a pseudo color scale, were overlayed with baboon's brain MR images (in gray scale).

Baboon PET Imaging

High, rapid, heterogeneous uptake of radioactivity into the baboon brain was observed during 3 baseline ^{18}F-FNDP PET scans in 3 different animals (Fig. 6). The regional distribution of ^{18}F-FNDP in the baboon brain agrees with the semiquantitative assessment of sEH expression in human (*2*) and mouse brain (*3*). The regional time–activity curves confirmed characteristics of optimally reversible PET radioligand binding. Notably, the washout rate of ^{18}F-FNDP in the baboon brain (Fig. 4) was less rapid than that in the mouse brain (Table 1) and was robust for mathematical modeling.

Blocking PET studies demonstrated that ^{18}F-FNDP labeled sEH in the baboon brain with very high specificity (Figs. 5 and 6; Supplemental Fig. 3). Blocking was observed in all baboon brain regions investigated, including the cerebellum.

sEH inhibitors can increase peripheral vasodilation and reduce blood pressure, which may, in turn, increase cerebral blood flow and affect radiotracer delivery. To examine that

possibility, we modeled radiotracer kinetics using the classic 2-tissue-3-compartment model from which the rate constant for transfer from arterial plasma to tissue (K_1) can be reliably estimated, in addition to the Logan graphical analysis. We found that whereas the V_T estimates were comparable between the compartmental modeling and the Logan method, the average K_1 values at baseline and blocking were 0.18 and 0.14 mL/cm^3/min, respectively, a 23% difference. That observation demonstrated that the K_1 changes cannot be attributed as the source for the marked reductions (>90%) of V_T values from baseline to blocking, confirming that ^{18}F-FNDP labeled sEH in the baboon brain with very high specificity. Our study did not reveal a reference region in the baboon brain that was nondisplaceable and free of sEH binding, in agreement with broad abundance of sEH in the mammalian brain (*2*,*3*).

The analysis of radiometabolites in baboon plasma demonstrated that ^{18}F-FNDP was metabolized to 2 hydrophilic radiometabolites. By the end of the 90-min PET scan, the remaining parent ^{18}F-FNDP represented approximately 20% of the radioactivity in plasma, comparable to many other PET radiotracers. Because the radiometabolites were hydrophilic, they are unlikely to enter the brain to an appreciable extent, simplifying the quantification of sEH in vivo.

CONCLUSION

We have developed ^{18}F-FNDP, the first specific PET radiotracer for imaging of sEH. ^{18}F-FNDP, a potent sEH inhibitor, readily entered the mouse (5 %ID/g tissue) and baboon (SUV = 4) brain and radiolabeled sEH with high specificity (up to 95%) in both animal species while exhibiting reversible brain kinetics amenable to quantitative analysis. ^{18}F-FNDP holds promise for further preclinical studies and human PET imaging to evaluate the role of sEH in a variety of conditions and disorders including VCI, mild cognitive impairment, and stroke.

DISCLOSURE

The costs of publication of this article were defrayed in part by the payment of page charges. Therefore, and solely to indicate this fact, this article is hereby marked "advertisement" in accordance with 18 USC section 1734. Financial support for this work was provided by NIH grants NS089437, NS078026, AT007317, NS038684, and NS060703; a DoD grant GW130098; an AHA Mid-Atlantic Affiliate grant-in-aid 13GRNT15730001; a Postdoctoral Fellowship Award 15POST25090114 (XL); and, in part, by the Division of Nuclear Medicine and Molecular Imaging of Johns Hopkins University. No other potential conflict of interest relevant to this article was reported.

ACKNOWLEDGMENTS

We thank Paige Finley and James Engles for their assistance with animal experiments, Karen Edmonds for PET scanner operation, Alimamy Kargbo for HPLC analysis of radiometabolites, and Julia Buchanan for editorial help.

REFERENCES

1. Spector AA, Norris AW. Action of epoxyeicosatrienoic acids on cellular function. *Am J Physiol Cell Physiol.* 2007;292:C996–C1012.
2. Sura P, Sura R, Enayetallah AE, Grant DF. Distribution and expression of soluble epoxide hydrolase in human brain. *J Histochem Cytochem.* 2008;56:551–559.
3. Marowsky A, Burgener J, Falck JR, Fritschy JM, Arand M. Distribution of soluble and microsomal epoxide hydrolase in the mouse brain and its contribution to cerebral epoxyeicosatrienoic acid metabolism. *Neuroscience.* 2009;163:646–661.
4. Newman JW, Morisseau C, Hammock BD. Epoxide hydrolases: their roles and interactions with lipid metabolism. *Prog Lipid Res.* 2005;44:1–51.
5. Shen HC, Hammock BD. Discovery of inhibitors of soluble epoxide hydrolase: a target with multiple potential therapeutic indications. *J Med Chem.* 2012;55:1789–1808.
6. White L, Petrovitch H, Hardman J, et al. Cerebrovascular pathology and dementia in autopsied Honolulu-Asia Aging Study participants. *Ann N Y Acad Sci.* 2002;977:9–23.
7. Knopman DS, Parisi JE, Boeve BF, et al. Vascular dementia in a population-based autopsy study. *Arch Neurol.* 2003;60:569–575.
8. Nelson JW, Young JM, Borkar RN, et al. Role of soluble epoxide hydrolase in age-related vascular cognitive decline. *Prostaglandins Other Lipid Mediat.* 2014;113-115:30–37.
9. Iliff JJ, Alkayed NJ. Soluble epoxide hydrolase inhibition: targeting multiple mechanisms of ischemic brain injury with a single agent. *Future Neurol.* 2009;4:179–199.
10. Ingraham RH, Gless RD, Lo HY. Soluble epoxide hydrolase inhibitors and their potential for treatment of multiple pathologic conditions. *Curr Med Chem.* 2011;18:587–603.
11. Martini RP, Ward J, Siler DA, et al. Genetic variation in soluble epoxide hydrolase: association with outcome after aneurysmal subarachnoid hemorrhage. *J Neurosurg.* 2014;121:1359–1366.
12. Lee CR, North KE, Bray MS, et al. Genetic variation in soluble epoxide hydrolase (EPHX2) and risk of coronary heart disease: the Atherosclerosis Risk in Communities (ARIC) study. *Hum Mol Genet.* 2006;15:1640–1649.
13. Hung YW, Hung SW, Wu YC, et al. Soluble epoxide hydrolase activity regulates inflammatory responses and seizure generation in two mouse models of temporal lobe epilepsy. *Brain Behav Immun.* 2015;43:118–129.
14. Qin X, Wu Q, Lin L, et al. Soluble epoxide hydrolase deficiency or inhibition attenuates MPTP-induced parkinsonism. *Mol Neurobiol.* 2015;52:187–195.
15. Heiss WD. PET imaging in ischemic cerebrovascular disease: current status and future directions. *Neurosci Bull.* 2014;30:713–732.
16. Morris E, Chalkidou A, Hammers A, Peacock J, Summers J, Keevil S. Diagnostic accuracy of F amyloid PET tracers for the diagnosis of Alzheimer's disease: a systematic review and meta-analysis. *Eur J Nucl Med Mol Imaging.* 2016;43:374–385.
17. Couto PJ, Millis RM. PET imaging of epigenetic influences on Alzheimer's disease. *Int J Alzheimers Dis.* 2015;2015:575078.
18. Eldrup AB, Soleymanzadeh F, Taylor SJ, et al. Structure-based optimization of arylamides as inhibitors of soluble epoxide hydrolase. *J Med Chem.* 2009; 52:5880–5895.
19. Imig JD, Zhao X, Zaharis CZ, et al. An orally active epoxide hydrolase inhibitor lowers blood pressure and provides renal protection in salt-sensitive hypertension. *Hypertension.* 2005;46:975–981.
20. Hilton J, Yokoi F, Dannals RF, Ravert HT, Szabo Z, Wong DF. Column-switching HPLC for the analysis of plasma in PET imaging studies. *Nucl Med Biol.* 2000;27:627–630.
21. CNS radiotracer table. National Institutes of Health website. http://www.nimh.nih.gov/research-priorities/therapeutics/cns-radiotracer-table.shtml. Accessed July 7, 2016.
22. Horti AG, Raymont V, Terry GE. PET imaging of endocannabinoid system. In: Dierckx R, Otte A, De Vries EF, Van Waarde A, eds. *PET and SPECT of Neurobiological Systems.* Berlin-Heidelberg, Germany: Springer; 2014:251–319.
23. Gao Y, Kuwabara H, Spivak CE, et al. Discovery of (-)-7-methyl-2-exo-[3′-(6-[^{18}F]fluoropyridin-2-yl)-5′-pyridinyl]-7-azabicyclo[2.2.1]heptane, a radiolabeled antagonist for cerebral nicotinic acetylcholine receptor (Î±4Î²2-nAChR) with optimal positron emission tomography imaging properties. *J Med Chem.* 2008;51:4751–4764.
24. Sinal CJ, Miyata M, Tohkin M, Nagata K, Bend JR, Gonzalez FJ. Targeted disruption of soluble epoxide hydrolase reveals a role in blood pressure regulation. *J Biol Chem.* 2000;275:40504–40510.